1 # Solubility and Reactivity of HNCO in Water: Insights into

2 # HNCO's Fate in the Atmosphere

3

4 **N. Borduas[1], B. Place[1], G. R. Wentworth[1], J. P. D. Abbatt[1] and J. G. Murphy[1,*]**

5 [1]{Department of Chemistry, University of Toronto, Toronto, Ontario, Canada}

6 Correspondence to: J. G. Murphy (jmurphy@chem.utoronto.ca)

7

8 **Abstract**

9 A growing number of ambient measurements of isocyanic acid (HNCO) are being made, yet

10 little is known about its fate in the atmosphere. To better understand HNCO's loss processes

11 and particularly its atmospheric partitioning behavior, we measure its effective Henry's Law

12 coefficient K_H^{eff} with a bubbler experiment using chemical ionization mass spectrometry as the

13 gas phase analytical technique. By conducting experiments at different pH values and

14 temperature, a Henry's Law coefficient K_H of 26 ± 2 M atm^{-1} is obtained, with an enthalpy of

15 dissolution of -34 ± 2 kJ mol^{-1}, which translates to a K_H^{eff} of 31 M atm^{-1} at 298 K and at pH 3.

16 Our approach also allows for the determination of HNCO's acid dissociation constant, which

17 we determine to be $K_a = 2.1 \pm 0.2 \times 10^{-4}$ M at 298 K. Furthermore, by using ion chromatography

18 to analyze aqueous solution composition, we revisit the hydrolysis kinetics of HNCO at

19 different pH and temperature conditions. Three pH dependent hydrolysis mechanisms are in

20 play and we determine the Arrhenius expressions for each rate to be $k_1 = (4.4 \pm 0.2) \times 10^7 \exp(-$

21 $6000 \pm 240 / T)$ M s^{-1}, $k_2 = (8.9 \pm 0.9) \times 10^6 \exp(-6770 \pm 450 / T)$ s^{-1} and $k_3 = (7.2 \pm 1.5) \times 10^8$

22 $\exp(-10900 \pm 1400 / T)$ s^{-1} where k_1 is for HNCO + H$^+$ + H$_2$O → NH$_4^+$ + CO$_2$, k_2 is for HNCO

23 + H$_2$O → NH$_3$ + CO$_2$ and k_3 is for NCO$^-$ + 2 H$_2$O → NH$_3$ + HCO$_3^-$. HNCO's lifetime against

24 hydrolysis is therefore estimated to be 10 days to 28 years at pH values, liquid water contents,

25 and temperatures relevant to tropospheric clouds, years in oceans and months in human blood.

26 In all, a better parameterized Henry's Law coefficient and hydrolysis rates of HNCO allow for

27 more accurate predictions of its concentration in the atmosphere and consequently help define

28 exposure of this toxic molecule.

1 Introduction

Until recently, the interest in studying HNCO was from a fundamental science perspective with research conducted on its structure, preparation and physical properties (Belson and Strachan 1982) and on its theoretical rovibrational spectra (Mladenović and Lewerenz 2008). Both theoretical and experimental data indicate that HNCO is the most stable CHNO isomer with a near-linear π-bond system (Hocking et al. 1975, Jones et al. 1950, Poppinger et al. 1977). In 2010, Roberts et al. reported detection of HNCO using negative ion proton transfer chemical ionization mass spectrometry (CIMS) from laboratory biomass burning and later determined its emission factor to be $0.25 - 1.20$ mmol per mol of CO for different types of biomass fuels (Veres et al. 2010). Shortly afterwards, the same authors reported the first ambient atmospheric measurements of HNCO in Pasadena, California, reaching 120 pptv and raising concerns of HNCO exposure due to its toxicity (Roberts et al. 2011). Indeed, HNCO has been observed to cause protein carbamylation leading to cardiovascular disease, rheumatoid arthritis and cataracts (Beswick and Harding 1984, Lee and Manning 1973, Mydel et al. 2010, Wang et al. 2007).

Since Roberts et al.'s initial measurements, ambient HNCO has also been measured in Boulder and in Fort Collins, Colorado, (Roberts et al. 2014), in Toronto, Ontario (Wentzell et al. 2013) and in Calgary, Alberta (Woodward-Massey et al. 2014). HNCO has also been detected simultaneously in the gas phase and in cloud water in La Jolla, California (Zhao et al. 2014). From these studies, typical urban concentrations range from below detection limits to approximately 100 pptv, whereas concentrations as high as 1.2 ppbv, enough to be of health concern, have been measured in air masses impacted by biomass burning in Boulder, Colorado (Roberts et al. 2011, Roberts et al. 2014, Woodward-Massey et al. 2014).

HNCO has a variety of anthropogenic and biogenic sources to the atmosphere. HNCO has been quantified from diesel engine exhaust (Kroecher et al. 2005, Wentzell et al. 2013) and light duty vehicles (Brady et al. 2014) as well as from biogenic sources such as biomass burning (Roberts et al. 2010, Roberts et al. 2011, Roberts et al. 2014, Veres et al. 2010). There also exist secondary sources of HNCO to the atmosphere, including the gas phase oxidation of amines and amides by OH radicals producing HNCO via H-abstraction mechanisms (Barnes et al. 2010, Borduas et al. 2013, Borduas et al. 2015). Evidence of secondary sources of HNCO has also been demonstrated in the field, with peak HNCO concentrations occurring during daytime (Roberts et al. 2011, Roberts et al. 2014, Zhao et al. 2014)
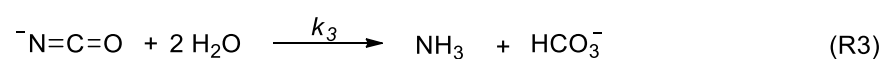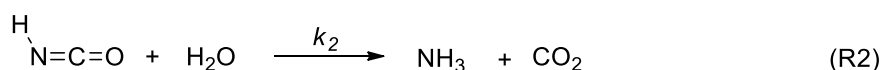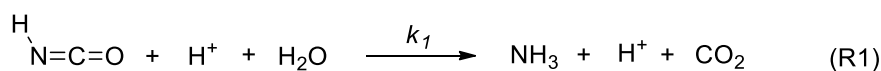
1   The sinks of HNCO however remain poorly constrained. HNCO has a lifetime of decades

2   towards OH radicals in the atmosphere as estimated by extrapolating high temperature rate

3   coefficients to atmospheric temperatures (Tsang 1992, Mertens et al. 1992, Tully et al. 1989).

4   It is also not expected to photolyze in the actinic region since its first UV absorption band is

5   observed below 280 nm wavelengths (Brownsword et al. 1996, Dixon and Kirby 1968, Rabalais

6   et al. 1969). Nonetheless, HNCO has served as a benchmark system in understanding

7   photodissociation decomposition pathways such as direct and indirect dissociation processes

8   and remains an area of active research (Yu et al. 2013) and references therein. HNCO is most

9   likely removed from the atmosphere by wet and/or dry deposition. HNCO's gas-to-liquid

10   partitioning is therefore an important thermodynamic property that can be used to predict its

11   atmospheric fate. Specifically, the Henry's Law coefficient K_H for the solubility of HNCO

12   represents the equilibrium ratio between its gas phase and aqueous phase concentrations at

13   infinite dilutions according to Eq. (1) (Sander 2015, Sander 1999). The Henry's Law coefficient

14   for HNCO has only recently been measured by Roberts and coworkers but their experimental

15   set up was limited to a single pH measurement (Roberts et al. 2011). As HNCO is a weak acid

16   with a pK_a of 3.7, its Henry's Law coefficient is expected to have a large pH dependence as

17   described in Eq. (2). Furthermore, the enthalpy of dissolution for HNCO is currently unknown.

18   In lieu of measurements, modelling studies on HNCO have used formic acid's enthalpy of

19   dissolution to model the temperature dependence of HNCO's Henry's Law coefficient (Barth

20   et al. 2013, Young et al. 2012). In our present study, we measure the effective Henry's Law

21   coefficient of HNCO at a range of pH and temperatures to determine its enthalpy of dissolution

22   for the first time.

23
$$K_H = {C_{HNCO}}/{p_{HNCO}} \tag{1}$$

24
$$K_H^{eff} = K_H \left(1 + \frac{K_a}{[H^+]} \right) \tag{2}$$

25   HNCO reacts irreversibly with water in the aqueous phase, an unusual property for an

26   atmospheric molecule. Once HNCO partitions to the aqueous phase, three mechanisms for its

27   hydrolysis are possible. The first (R1) is acid-catalysed and is therefore termolecular whereas

28   the second (R2) and third (R3) are bimolecular reactions involving either the protonated or

29   deprotonated form of HNCO (Scheme 1) (Amell 1956, Belson and Strachan 1982, Jensen

30   1958). In 1958, Jensen determined the hydrolysis rate of the three mechanisms through addition

31   of AgNO$_3$ to buffered solutions at different time points to precipitate unreacted isocyanate as

32   AgNCO, followed by back titration of excess AgNO$_3$ with NH$_4$SCN. Considering the

1 importance of these mechanisms in evaluating the fate of HNCO in the atmosphere, we follow

2 up on the study by Jensen with our own experiments using ion chromatography to determine

3 the pH and temperature dependencies of the overall rate of hydrolysis of HNCO. Quantitative

4 knowledge of the ability of HNCO to partition to the aqueous phase and its subsequent reactions

5 with water allows for an accurate understanding of the chemical fate of HNCO in the

6 atmosphere (Fig. 1). In this study, we therefore provide laboratory measurements of HNCO's

7 Henry's Law coefficient and enthalpy of dissolution as well as its three rates of hydrolysis and

8 their respective activation energies.

$$H-N=C=O + H^+ + H_2O \xrightarrow{k_1} NH_3 + H^+ + CO_2 \qquad (R1)$$

$$H-N=C=O + H_2O \xrightarrow{k_2} NH_3 + CO_2 \qquad (R2)$$

$$^-N=C=O + 2\,H_2O \xrightarrow{k_3} NH_3 + HCO_3^- \qquad (R3)$$

9

10 Scheme 1: The three mechanisms involved in HNCO's hydrolysis.
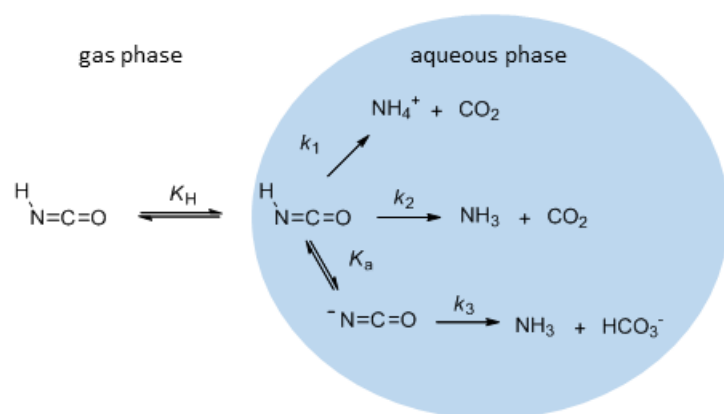

11

12 Figure 1: The fate of HNCO in the atmosphere includes its partitioning between the gas and

13 aqueous phases and its hydrolysis through three different mechanisms governed by k_1, k_2, and

14 k_3.

2 Experimental Methods

2.1 Henry's Law coefficient experiments

17 To measure the effective Henry's Law coefficient K_H^{eff} of HNCO, we use a bubbler column

18 experimental set up and detect HNCO through chemical ionization mass spectrometry.

2.1.1 Acetate reagent ion CIMS

The quadrupole chemical ionization mass spectrometer (CIMS) was built in house and is described in detail elsewhere (Escorcia et al. 2010). We opted to use acetate as the reagent ion which has been shown to be sensitive for the detection of acids (Roberts et al. 2010, Veres et al. 2008). For this experimental set up, the reagent ion was generated by flowing 20 sccm of nitrogen over a glass tube containing acetic anhydride (from Sigma-Aldrich and used as is) and maintained at 30 $^{\circ}$C. This flow was subsequently mixed with a nitrogen dilution flow of 2 L min^{-1} and passed through a polonium-210 radioactive source to generate acetate ions. All flows were controlled using mass flow controllers. The data acquisition was done under selected ion mode where 10 m/z ratios were monitored with dwell times of 0.2 s each and each duty cycle was 4 s. Ions measured included m/z 59 (AcO-), m/z 119 ((AcOH)AcO-), m/z 51 (black counts), m/z 35 (Cl-), m/z 42 (NCO-), m/z 45 (HCOO-), m/z 46 (ONO-), m/z 96, m/z 102 and m/z 113. The raw signals are then normalized to m/z 59 and reported as normalized counts per second (ncps). For the exception of m/z 42, none of the ions were observed to change during the experiments. The inlet flow of the CIMS is governed by a pin hole at 0.5 L min^{-1}, and a N$_2$ dilution flow of 0.4 L min^{-1} into the inlet was used to avoid depletion of the acetate reagent ion by high HNCO concentrations. Previous work suggests there is no significant role of water vapour in HNCO's detection by acetate CIMS (Roberts et al. 2010). With the CIMS's inlet dilution, the RH within the ion molecule region was < 20%.

2.1.2 Experimental set up for measurement of K_H

To obtain the Henry's Law coefficient, K_H, we monitored the decrease in gas phase HNCO exiting a buffered aqueous solution for a range of volume flow rates. A bubbler column experimental set up is used with online gas phase detection. This method is employed to measure HNCO's partitioning and take into account the concurrent hydrolysis of HNCO in the buffer solution at high time resolution. Our experimental setup is based on previous work (Kames and Schurath 1995, Roberts 2005, Roberts et al. 2011) and our apparatus is comprised of one fritted bubbler with an approximate volume of 70 mL which contained 15 mL of a citric acid/Na$_2$HPO$_4$ buffer at varying pH. The 15 mL volume was chosen to reduce HNCO equilibration times and to simultaneously ensure that the bubbler's frit was submerged. Experiments performed in 30 mL of buffer yielded identical results. The water lost to the gas phase during the experiments (< 1 h) was at most 5% of the original buffer volume and so no corrections to the latter were required. The bubbler was held in a temperature-controlled bath

5

of approximately 1:1 mixture of deionized water and ethylene glycol. Upstream of the bubbler, where the RH was measured to be ~ 50%, was a valve and a tee connection where the dry HNCO flow could be connected and disconnected during the experiments. Downstream of the bubbler was another tee which connected to both the exhaust and the acetate reagent ion CIMS. Conveniently, the absolute concentration of gas-phase HNCO is not required in this approach since it relies on the decay of the signal, $[HNCO]_t/[HNCO]_0$ and not on the absolute gas phase and aqueous phase concentrations.

HNCO was produced using a permeation source which sublimes solid cyanuric acid at 250 ^{o}C in a flow of dry nitrogen and is described in detail elsewhere(Borduas et al. 2015). This source is based on HNCO sublimation techniques and on a similar source previously developed by Roberts et al. (Belson and Strachan 1982, Roberts et al. 2010). The buffer solutions were made with solid citric acid, disodium phosphate and deionized water with citric acid concentrations ranging from 0.02 M to 0.0035 M to access a pH range of 2.5-4.0.

Each experiment began with gaseous HNCO flowing through a fresh buffer solution until a reasonably stable signal (> 0.01 ncps) was obtained by the CIMS (background counts ~ 5×10^{-4} ncps). The solution did not need to reach equilibrium for the experiment to proceed and so lower temperatures and higher pHs (when the equilibration time is longest and may reach over 4-5 hours) were feasible. Once a normalized signal (i.e. relative to the reagent ion signal) of at least 0.025 for HNCO was obtained, the flow of HNCO through the bubbler was turned off, and only pure nitrogen continued to flow through. The HNCO signal then decayed exponentially as a function of time due to partitioning as well as hydrolysis. This decay was monitored until it had decreased to less than one quarter of the original signal. This method also has the advantage of extracting an effective Henry's Law coefficient without needing to monitor the aqueous phase HNCO concentration.

2.2 Hydrolysis rate experiments

HNCO in the aqueous phase was measured using ion chromatography at different pH and temperatures to determine its rates of hydrolysis.

2.2.1 Ion chromatography

The measurements for the hydrolysis of HNCO were made using a Dionex IC-2000 Ion Chromatography (IC) System. An IonPac (AS19) anion column consisting of a quaternary

ammonium ion stationary phase with diameter and length dimensions of 4 mm and 25 mm respectively was employed. Sample runs used a concentration gradient of the eluent KOH ranging from 2 mM to 20 mM. An optimized elution program was written for each pH range measured (between 25-60 minutes for each injection). Samples were injected using a Dionex (AS40) automated sampler into a 25 µL loop for pre-injection. The use of a loop rather than a concentrator was important and ensured that the total $HNCO/NCO^-$ concentrations were being measured. The IC was calibrated using matrix-matched standards of known $HNCO/NCO^-$ concentrations prepared from serial dilutions of KOCN (Sigma-Aldrich, 96% purity).

2.2.2 Hydrolysis kinetics experiments

The kinetics of the hydrolysis reactions in the pH range of 1-2 are very fast; complete decays occurred in a matter of minutes. The decay of HNCO at these low pH values is therefore too quick for the 25 min IC method to capture. To circumvent this issue, we used a quenching method. Specifically, we prepared an aqueous solution of 50 mL of sulphuric acid at the desired pH. 5 mL of this acidic solution was subsequently added to a 0.02 M solution of KOCN in eight different falcon tubes to initiate the rapid hydrolysis reaction. Each reaction was then quenched at different times by a 0.1 M aqueous solution of KOH. Increasing the pH to more than 10 slowed the hydrolysis kinetics by orders of magnitude and allowed for subsequent IC measurements. Replacing sulphuric acid by nitric acid and/or KOH by NaOH yielded identical hydrolysis rates and ensured the results were reproducible with different acids and bases.

Buffer solutions in the pH range of 3-5 were prepared by using appropriate molar ratios of citric acid and disodium phosphate whereas buffer solutions in the pH range of 9-10 used sodium carbonate and sodium bicarbonate. All buffer concentrations were < 0.002 M, and we assume that the ionic strength of these solutions had minimal impact on the solubility of HNCO. For the room temperature set of kinetic experiments, the experiment was initiated by the addition of 0.1 g of KOCN to 50 mL of the desired buffer solution. The solution was further diluted by a factor of 500 and then split into 8 samples for analysis at succeeding intervals on the anion IC.

Hydrolysis reactions were run at different temperatures to assess the activation energies of each of the three hydrolysis mechanisms. Room temperature reactions were conducted inside the IC autosampler AS40 (with a cover) and monitored by a temperature button (iButtons, Maxim Integrated, San Jose, CA with 0.5 °C resolution)). Colder temperature reactions were done in a

1 water ice bath and monitored by a thermometer. Finally, warmer temperature reactions for high

2 pH samples were run in a temperature-controlled water bath. These reactions took days to

3 weeks to reach completion, and so 5 mL samples from the reaction mixtures were taken out of

4 the water bath and measured on the IC at appropriate time intervals.

5 ## 3 Results and Discussion

6 ### 3.1 Henry's Law coefficient K_H

7 HNCO's effective Henry's Law solubility coefficient K_H^{eff} expressed in M atm^{-1} was determined

8 based on the exponential decay of gaseous HNCO exiting a bubbler containing a buffered

9 solution. The observed decay of HNCO is caused by its partitioning from the aqueous phase to

10 the gas phase as well as its competing hydrolysis reaction. Equation (3) represents the rate law

11 for the disappearance of HNCO during the experiment and Eq. (4) is the integrated rate law.

12
$$-\frac{d[HNCO]}{dt} = [HNCO]\frac{\varphi}{K_H^{eff}VRT} + [HNCO]k_{hyd} \tag{3}$$

13
$$ln\frac{[HNCO]_t}{[HNCO]_0} = -\left[\frac{\varphi}{K_H^{eff}VRT} + k_{hyd}\right]t \tag{4}$$

14 Where $[HNCO]_t$ is the HNCO concentration at time t, $[HNCO]_0$ is the initial HNCO

15 concentration (at time $t = 0$), $[HNCO]_t/[HNCO]_0$ is the HNCO concentration in the gas phase

16 downstream of the bubbler measured by the CIMS, φ is the volumetric flow rate (cm^3 s^{-1}), K_H^{eff} is

17 the effective Henry's Law coefficient for solubilty (mol L^{-1} atm^{-1}), V is the liquid volume of the

18 buffer (cm^3), R is the ideal gas constant (8.21×10^{-2} L atm mol^{-1} K^{-1}), T is the temperature (K),

19 k_{hyd} is HNCO's overall rate of hydrolysis (s^{-1}) and t is the time (s). To extract the value of K_H^{eff}

20 from the experimental decay curves, we first plot the natural logarithm of change in HNCO

21 concentration versus time for different flow rates ranging from 175 to 800 sccm as shown in

22 Fig. 2A. The slope of each experiment is then plotted as function of the ratio of the flow rate

23 and volume depicted in Fig. 2B. The slope of Fig. 2B leads to a value representing $(K_H^{eff}RT)^{-1}$
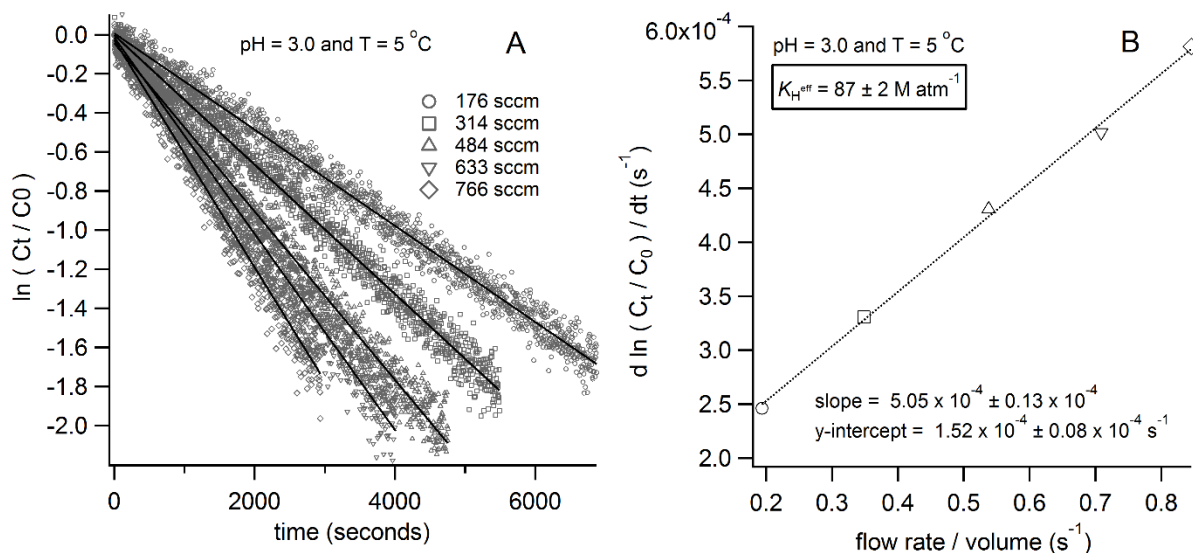
24 and so K_H^{eff} can be calculated.

1

Figure 2: A) The concentration decay curves as a function of time according to Eq. (4) for each flow rate shown; B) The slopes of each fit in Fig. 2A plotted as a function of the ratio of the flow rate to the volume. The symbols in both figures represent the same flow rate shown.

These dynamic experiments were repeated with a range of buffer solutions ranging from pH 2.5-4.0 to determine the pH-independent Henry's Law coefficient, K_H, of HNCO. Experiments at temperatures of 273-298 K were also conducted to determine HNCO's enthalpy of dissolution, ΔH_{diss}.

3.1.1 pH dependence of K_H^{eff}

The pH dependence of the effective Henry's Law coefficient K_H^{eff} of a weak acid like HNCO depends on its pK_a as well as on the pH according to Eq. (2). Throughout our experiments, we measure the value of K_H^{eff} and employ Eq. (2) to plot K_H^{eff} as a function of the inverse of the proton concentration, [H^+], and thus to extract HNCO's Henry's Law coefficient for solubility, K_H. Figure 3A depicts this linear relationship and yields a value of 26 ± 2 M atm^{-1} for K_H. Our K_H value compares well with the only other published value of 21 M atm^{-1} determined solely at pH 3 (Roberts et al. 2011). Figure 3B on the other hand shows experimentally determined K_H^{eff} at different pH values and at a constant temperature of 298.0 ± 0.2 K. Error bars in both Fig. 3A and 3B represent the percentage of the standard deviation of the slope as in Fig. 2B. The slope in Fig. 3A also allows us to determine HNCO's acid dissociation constant, K_a, which at 298 K is $2.1 \pm 0.2 \times 10^{-4}$ M. Our K_a value also agrees well with previously reported K_a for HNCO (Amell 1956, Belson and Strachan 1982).
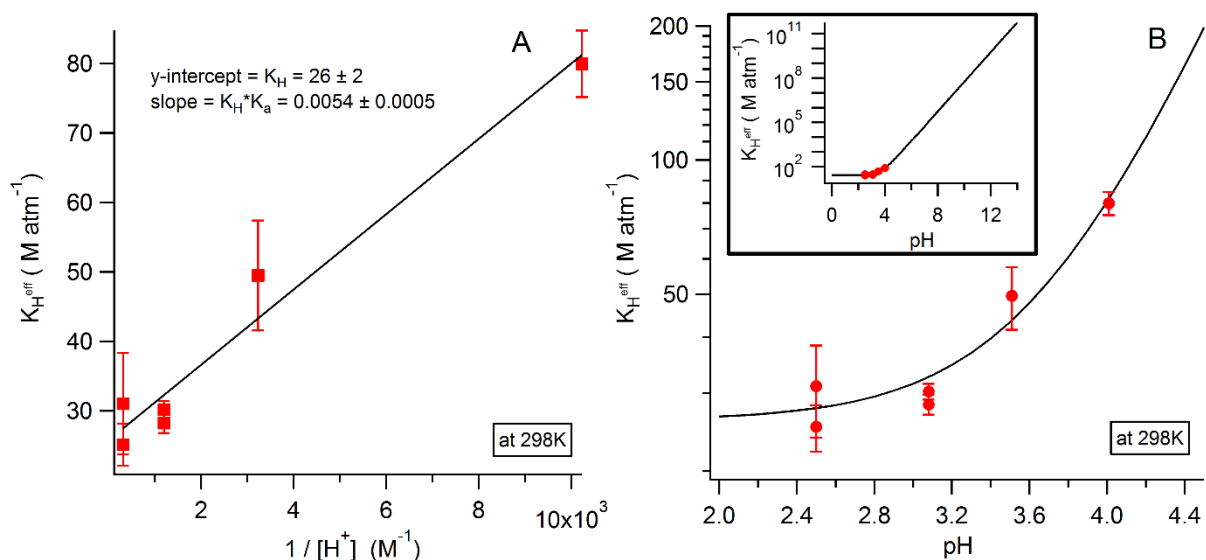
9

Figure 3: A) The fit according to Eq. (2) of the experimental K_H^{eff} values which allows for the determination of K_H and K_a at 298 K. B) The experimental K_H^{eff} values as a function of pH at 298 K. The black line is the modelled dependence of K_H^{eff} according to Eq. (2) based on the determined value of K_H and a value for K_a of 2.1×10^{-4} M. The inset shows the range of K_H^{eff} across the full range of pH.

3.1.2 Temperature dependence

The temperature dependence of HNCO's solubility was established by running experiments at varying temperatures from 273 to 298 K. Since K_H^{eff} is very sensitive to pH changes, all experiments were conducted with a buffer solution from the same batch and same volumetric flask within a few days. Plotting the natural logarithm of the effective Henry's Law coefficient as a function of the inverse of temperature yields the ratio of the enthalpy of dissolution, ΔH_{diss}, to the gas constant, R (Fig. 4). We report a value of -34 ± 2 kJ mol^{-1} for HNCO's enthalpy of dissolution, where the uncertainty stems from the deviation from the slope depicted in Figure 4. This value compares to similar weak acids like HONO (-40 kJ mol^{-1}) and HCN (-42 kJ mol^{-1}), but differs from the value of formic acid (-47 kJ mol^{-1}) which was the value assumed for HNCO in the Young et al. and the Barth et al. modelling studies (Barth et al. 2013, Sander 2015, Young et al. 2012).
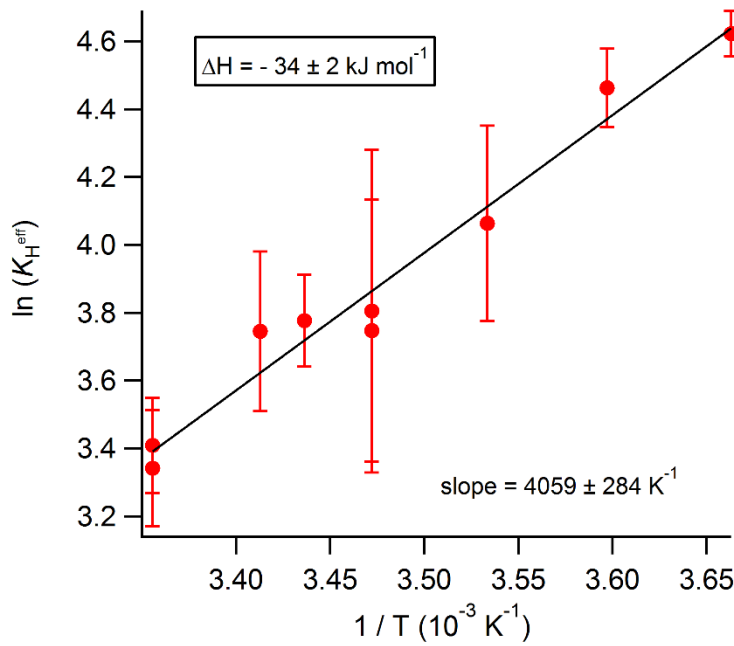
Figure 4: The temperature dependence of experimentally measured K_H^{eff} at pH 3.08.

3.2 Rate of hydrolysis k_{hyd}

There are three mechanisms by which HNCO can react with water described in Scheme 1 (R1) to (R3) and depicted in Fig. 1. The disappearance of HNCO in the aqueous phase can therefore be described by the rate law shown as Eq. (5). The pH dependence of HNCO's hydrolysis manifests itself in the first term of Eq. (5) as the hydrogen ion concentration as well as in the concentration of the dissociated/non-dissociated acid in each term.

$$-\frac{d[HNCO]_t}{dt} = k_1[HNCO][H^+] + k_2[HNCO] + k_3[NCO^-] \tag{5}$$

To mathematically integrate this rate law, the concentration of HNCO needs to be expressed as the sum of undissociated HNCO and of isocyanate ion NCO⁻ in solution, which is denoted in Eq. (6) as [HNCO]$_{tot}$. HNCO's acid dissociation constant K_a relates the concentration of HNCO and NCO⁻ as shown in Eq. (6). The K_a-dependant expression of Eq. (6)is then substituted into the rate law of Eq. (5), and subsequently integrated. The K_a value of HNCO has a slight temperature dependence with a heat of dissociation previously measured to be 5.4 kJ mol⁻¹, which for the temperature range of 273 to 298 K represents a 25% change (Amell 1956). We therefore use Amell's heat of dissociation value throughout our analysis to account for K_a's temperature dependence in the van't Hoff equation. Furthermore, Belson et al.'s evaluation of the K_a of HNCO literature recommends 2.0×10^{-4} M at 298 K (Belson and Strachan 1982).

1 Finally, our own work on the pH dependence of Henry's Law coefficient of HNCO, suggests a

2 K_a value of $2.1 \pm 0.2 \times 10^{-4}$ M at 298 K, consistent with the recommended value (Fig. 3A).

3
$$[HNCO] = [HNCO]_{tot} - [NCO^-] = \frac{[H^+][NCO^-]}{K_a} = \frac{[HNCO]_{tot}[H^+]}{K_a + [H^+]} \qquad (6)$$

4 By integrating Eq. (5) with the appropriate substitutions, the resulting expression is Eq. (7),

5 where k_{hyd} represents the observed first-order rate loss of hydrolysis of HNCO and depends on

6 the individual reaction rates k_1, k_2 and k_3 according to Eq. (8).

7
$$\frac{[HNCO]_t}{[HNCO]_0} = e^{-k_{hyd}t} \qquad (7)$$

8
$$k_{hyd} = \frac{k_1[H^+]^2 + k_2[H^+] + k_3 K_a}{K_a + [H^+]} \qquad (8)$$

9 The aim of our hydrolysis experiments is to measure k_{hyd} at different pH values to subsequently

10 solve for the values of the individual hydrolysis rate coefficients k_1, k_2 and k_3. To measure k_{hyd},

11 we employ ion chromatography (IC) which allows for quantitative measurement of the total

12 isocyanic acid in solution as NCO$^-$ using an anion chromatography column. The key to making

13 [HNCO]$_{tot}$ measurements was to use a loop injection port for the IC instead of a concentrator

14 column, since the latter retains only ions and would not measure any protonated HNCO in

15 solution. Appropriate buffer solutions were made to conduct experiments over a range of pH

16 values from 1.7 to 10.4. The decay of [HNCO]$_{tot}$ was monitored by IC over time and plotting

17 the natural logarithm of the decay as a function of time as in Fig. 5 yields the k_{hyd} specific to

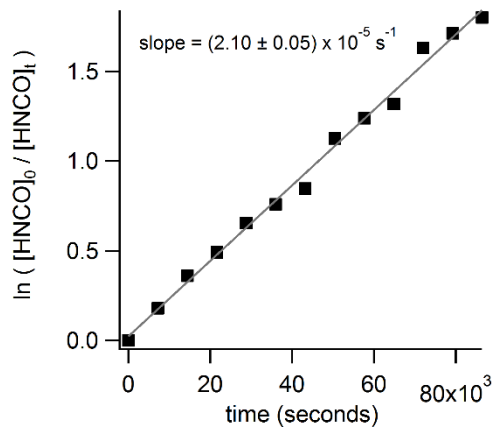18 that temperature and pH. Hydrolysis experiments are listed in Table A1 in Appendix A.

19

20

21 Figure 5: Example of a hydrolysis experiment at pH 5.4 and at 25 °C where the [HNCO]$_{tot}$ is

22 measured by loop injections on the IC.

3.2.1 Determining k_1 and k_2

At a pH below 3, the third hydrolysis mechanism (Scheme 1 (R3)) will contribute minimally to the overall k_{hyd}. Indeed, the third term in Eq. (8), $k_3 K_a/(K_a+[H^+])$ will become very small because $[H^+] \gg K_a$. Furthermore, very little of the HNCO is present as NCO$^-$ at low pH. This assumption (which we verify retroactively) simplifies the k_{hyd} expression to Eq. (9) with only two unknowns, k_1 and k_2. We can now solve for k_1 and k_2 from two k_{hyd} values derived from experiments conducted at two different pH values but at the same temperature. For example, solving for k_1 and k_2 at 295 K using the k_{hyd} in Table A1, we obtain a value of $(6.73 \pm 0.27) \times 10^{-2}$ M s^{-1} for k_1 and of $(1.04 \pm 0.04) \times 10^{-3}$ s^{-1} for k_2. We do this calculation once per temperature. The uncertainties associated with these measurements come from the slope of decay of aqueous phase HNCO measured by IC.

$$k_{hyd@pH<2.7} = \frac{k_1[H^+]^2+k_2[H^+]}{K_a+[H^+]} \tag{9}$$

3.2.2 Temperature dependence of k_1 and k_2

Hydrolysis experiments of HNCO at three different temperatures further enables us to solve for the temperature dependence of k_1 and k_2. We chose three temperatures relevant to tropospheric air masses: 270, 283 and 295 K. Figure 6 represents the slope of the natural logarithm of the rate coefficient of hydrolysis as a function of the inverse of the temperature which according to the Arrhenius equation shown in Eq. (10) yields the activation energy specific to each hydrolysis mechanism. We obtain activation energies of 50 ± 2 kJ mol^{-1} and 56 ± 4 kJ mol^{-1} for k_1 and k_2 respectively. Furthermore, the y-intercept of these linear plots yields the value of ln(A) in Eq. (10) and so the A factors of each hydrolysis mechanism can also be obtained, providing Arrhenius expressions of $k_1 = (4.4 \pm 0.2) \times 10^7 \exp(-6000 \pm 240 / T)$ M s^{-1} and $k_2 = (8.9 \pm 0.9) \times 10^6 \exp(-6770 \pm 450 / T)$ s^{-1}. The uncertainties stem from the fit to the data points in Figure 6 (and their error bars comes from the slope of the decay of aqueous phase HNCO measured by IC).
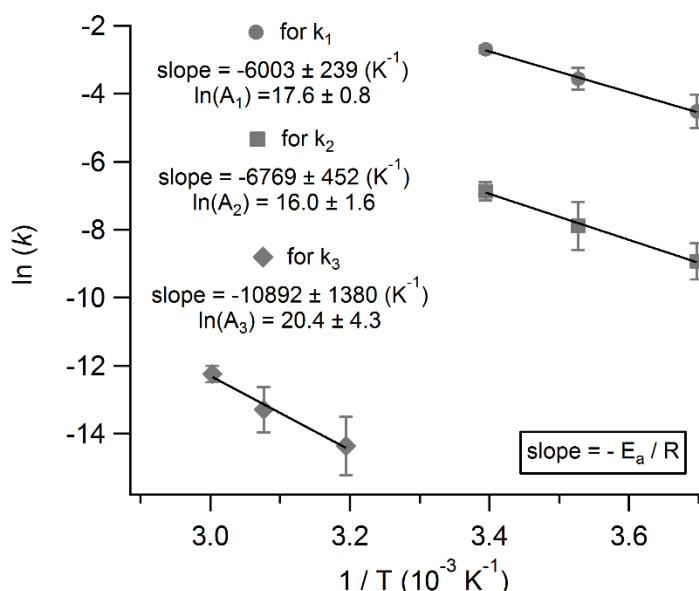
$$k = Ae^{-E_a/RT} \tag{10}$$

Figure 6: The linear plots of the natural logarithm of each hydrolysis rate coefficient k_1, k_2 and k_3 as a function of the inverse of temperature to yield the activation energies of each mechanism.

3.2.3 Determining k_3 and its temperature dependence

At high pH levels, the third hydrolysis mechanism (Scheme 1 (R3)) will dominate the observed $k_{hyd,}$ however, the first two mechanisms may still have a non-negligible contribution to k_{hyd} and can therefore not be disregarded. We can solve for k_3, knowing k_1 and k_2 and their respective temperature dependencies, using Eq. (8). The k_{hyd} values measured at pH above 9 and at 40 °C are used (Table A1), and k_3 is determined for each pH. The average of our three measurements at 40 °C is $(5.77 \pm 0.35) \times 10^{-7}$ s^{-1}. The temperature dependence of k_3 is determined in an analogous way to k_1 and k_2 and is also depicted in Fig. 6. We obtain a value of 91 ± 12 kJ mol^{-1} which translates to an Arrhenius expression of $k_3 = (7.2 \pm 1.5) \times 10^8 \exp(-10900 \pm 1400 / T)$ s^{-1}.

Equipped with the values of k_1, k_2 and k_3 and their temperature dependencies, a map of the expected total hydrolysis rate, k_{hyd}, as a function of temperature and pH can be generated using Eq. (8) and Eq. (10) and is plotted as Fig. 7. For reference, the colour scale of Fig. 7 also reads in hydrolysis lifetime of HNCO in hours. It is clear that HNCO's lifetime in the aqueous phase has a large temperature and pH dependence.

3.2.4 Comparing the rate of hydrolysis k_{hyd} through different methods

The individual rate coefficients of the three hydrolysis mechanisms (Scheme 1 (R1) to (R3)) have only been evaluated one other time in the literature (Jensen 1958). Our IC experimental method differs substantially from Jensen's back titration method, and yet we obtain similar values for k_1, k_2 and k_3 as well as for their respective activation energies. The values are summarized in Table 2. Again, the colour scale of Fig. 7 is generated from Eq. (8) using our obtained values for k_1, k_2 and k_3 and for E_{a1}, E_{a2} and E_{a3}, and we superimpose all our k_{hyd} measurements from Table A1 as circles. We further add Jensen's published raw data for comparison (Jensen 1958) as triangles. The agreement is good and is consistently within the same order of magnitude (Fig. 7).

Table 2: HNCO's Henry's Law coefficient, acid dissociation constant and hydrolysis constants

Physical parameter	Value	Energy	Reference
Henry's Law coefficient, K_H	26 ± 2 M atm^{-1}	$\Delta H_{diss} = -34 \pm 2$ kJ mol^{-1}	This work
	21 M atm^{-1}	–	Roberts et al. 2011
Acid dissociation constant, K_a^*	$2.1 \pm 0.2 \times 10^{-4}$ M	–	This work
	2.0×10^{-4} M	$\Delta H_{diss} = -5.4$ kJ mol^{-1}	Amell 1956
Hydrolysis rate coefficient, k_1^*	$7.6 \pm 0.3 \times 10^{-2}$ s^{-1}	$E_{a1} = +50 \pm 2$ kJ mol^{-1}	This work
	1.1×10^{-1} s^{-1}	$E_{a1} = +63$ kJ mol^{-1}	Jensen 1958
Hydrolysis rate coefficient, k_2^*	$1.4 \pm 0.1 \times 10^{-3}$ s^{-1}	$E_{a2} = +56 \pm 4$ kJ mol^{-1}	This work
	1.8×10^{-3} s^{-1}	$E_{a2} = +83$ kJ mol^{-1}	Jensen 1958
Hydrolysis rate coefficient, k_3^*	$8.1 \pm 1.7 \times 10^{-8}$ s^{-1}	$E_{a3} = +91 \pm 12$ kJ mol^{-1}	This work
	1.2×10^{-8} s^{-1}	$E_{a3} = +100$ kJ mol^{-1}	Jensen 1958

* at 298 K

In addition, our Henry's Law coefficient experiment provides a complimentary way to determine k_{hyd} at different temperatures and pH values. Indeed, the intercept of the line which fit the data of $d\ln(C_t/C_0)/dt$ versus φ/V yields k_{hyd}, representing the value for the loss process in the solution of the bubbler column experiment (an example is given in Fig. 2B). We show these values as squares in Fig. 7. Roberts et al. also determined k_{hyd} through this method at pH 3 and

1   at 25 ºC and this value is appended to Fig. 7 (Roberts et al. 2011) as a diamond. The agreement

2   is good from all four cases. We can conclude that the lifetime of HNCO against hydrolysis in

3   dilute aqueous solutions spans seconds to years depending on pH and temperature. The lifetime

4   of HNCO against hydrolysis in cloud water of pH 3-6 will be shorter and range from 10 hours

5   to ~20 days in the troposphere. On the other hand, HNCO's hydrolysis in ocean waters of pH

6   ~8.1 and temperatures below 30 ºC will be very slow, translating to a lifetime of 1-2 years if

7   we assume no other reactive chemistry is taking place. Finally, in the context of exposure, if

8   HNCO is present in human blood at physiological pH and temperature, its lifetime to hydrolysis

9   will be as high as several months. On the other hand, if HNCO is present in the stomach, which

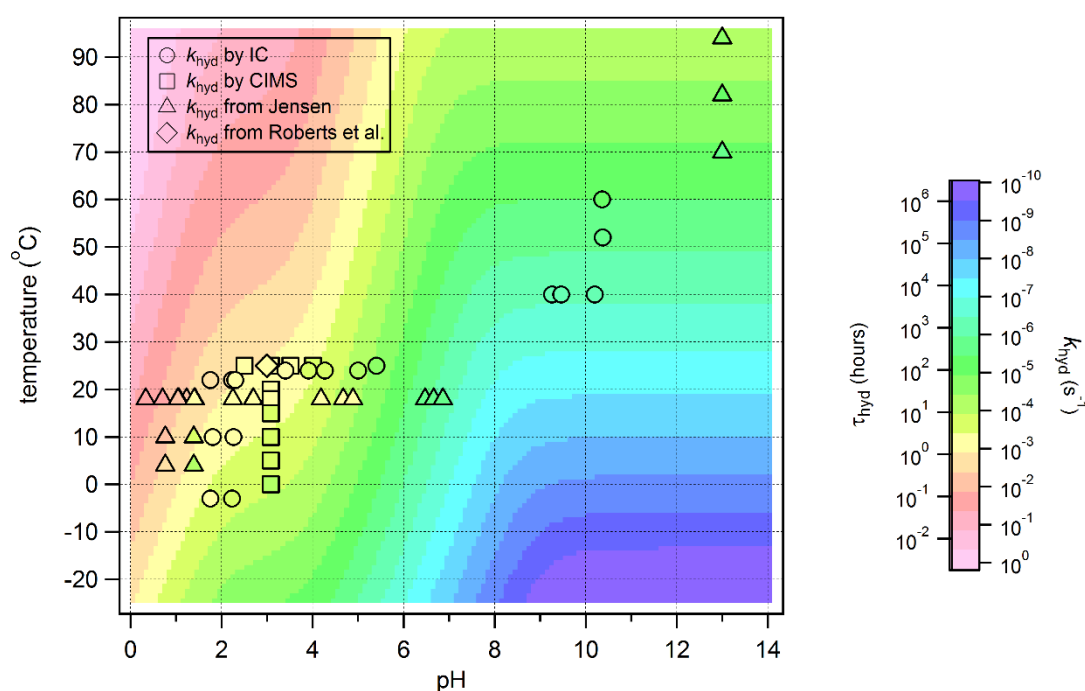10 is more acidic, we would expect its lifetime to drop to minutes or hours.

11

12 Figure 7: k_{hyd} as function of temperature and pH generated from Eq. (8) using our obtained

13 values for k_1, k_2 and k_3 and for E_{a1}, E_{a2} and E_{a3}. All available k_{hyd} measurements for HNCO in

14 the literature and from this work are superimposed and colour coded appropriately. As a guide,

15 the colour scale also represents the lifetime in hours for HNCO in dilute aqueous solutions.

16 **4   Atmospheric Implications**

17 HNCO is a toxic molecule and can cause cardiovascular and cataract problems through protein

18 carbamylation (Beswick and Harding 1984, Mydel et al. 2010, Wang et al. 2007). Recently

19 reported ambient measurements of HNCO in North America raise concerns of exposure

20 particularly from biomass burning, diesel and gasoline exhaust and urban environments (Brady

1 et al. 2014, Roberts et al. 2011, Roberts et al. 2014, Wentzell et al. 2013, Woodward-Massey

2 et al. 2014, Zhao et al. 2014). With the values for HNCO's Henry's Law coefficient and

3 hydrolysis rates reported here, a better understanding of HNCO's removal rate from the

4 atmosphere can be determined, and hence HNCO's atmospheric lifetime can be estimated. Note

5 however that our HNCO lifetime estimates do not consider dry deposition and therefore

6 represent a higher limit, particularly since Young et al. found that dry deposition can be

7 significant for HNCO (Young et al. 2012).

8 Specifically, the lifetime of HNCO in the atmosphere will depend on its partitioning to the

9 aqueous phase K_H^{eff}, the temperature T, the pH and liquid water content (LWC) of the

10 aerosol/droplet and finally the hydrolysis of HNCO k_{hyd} once in solution. We can calculate

11 HNCO's lifetime against hydrolysis based on Eq. (11) where τ is the lifetime in seconds, L is

12 the fraction of air volume occupied by liquid water (dimensionless) and R is the gas constant.

13 Figures 8A and 8B depict outputs of Eq. (11) with different fixed variables. Figure 8A holds

14 the LWC to 1 g m^{-3}, a value representative of cloud water, highlighting the dependence of

15 HNCO's lifetime on temperature and pH (Ip et al. 2009). At atmospherically relevant pH of 2

16 to 6 and at temperatures below 30 ^{o}C, HNCO has a lifetime on the order of 10 days to hundreds

17 of years. Alternatively, Fig. 8B holds the pH at 4 and varies the LWC on the x-axis. Water

18 concentrations relevant to wet aerosol (1-100 μg m^{-3}) are too small to act as a significant sink

19 for gas phase HNCO. However, Fig. 8B highlights the strong dependence of HNCO lifetime

20 on LWC in clouds, again ranging from days to hundreds of years. It therefore appears that if

21 HNCO is incorporated into cloud water, it is more likely to be rained out or revolatilized than

22 to hydrolyse given typical times in clouds of minutes to hours. There is also the possibility that

23 HNCO has other currently unknown sinks in cloud water that may be competitive with its

24 hydrolysis and further work on HNCO's aqueous phase chemistry with nucleophiles such as

25 amines and alcohols is currently underway in our laboratories.Finally, HNCO will partition

26 readily in oceans at pH ~8, but will take years to hydrolyze.

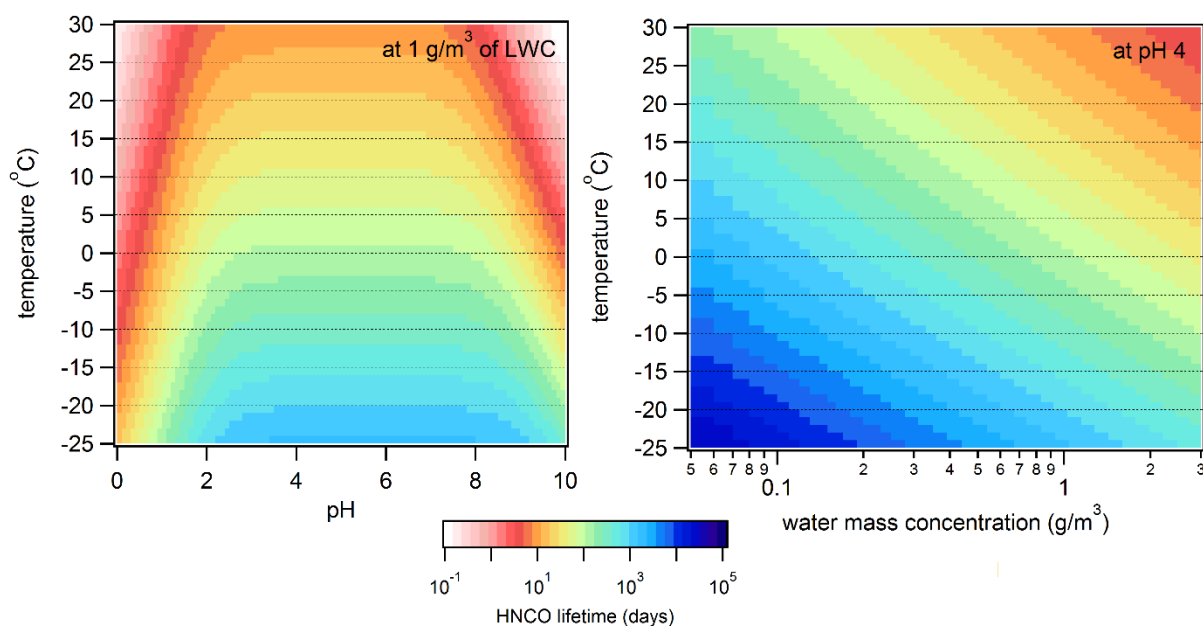27 $$\tau = 1/K_H^{eff} RTLk_{hyd} \tag{11}$$

Figure 8: A) The lifetime of HNCO in days as a function of temperature and pH at 1 g m^{-3} of LWC and B) the lifetime of HNCO in days as a function of temperature and LWC at pH 4

Zhao et al. (2014) observed higher concentrations of HNCO in the cloud water in La Jolla, California than predicted by its Henry's Law coefficient at 298 K(Zhao et al. 2014)(Zhao et al. 2014)(Zhao et al. 2014). This observation remains puzzling but may point towards sources of HNCO within cloud water other than simple partitioning chemistry. The Barth et al. 2013 modeling study concluded that fog, low-level stratus clouds or stratocumulus clouds were the most efficient cloud conditions at removing HNCO from the gas phase, particularly in polluted scenarios where the cloud water was more acidic. The authors highlighted the high dependence of HNCO's fate on liquid water pH and temperature, consistent with our findings (Barth et al. 2013). The Young et al. 2012 study, which modelled global HNCO budgets, assumed the aqueous loss of the weak acid occurred only when the cloud liquid water content was greater than 1 mg m^{-3}. Based on Fig. 8B, 1 mg m^{-3} is low for HNCO to significantly partition into the aqueous phase and rather requires water mass concentrations 1000 times greater for HNCO's lifetime to drop to days. The model may have overestimated the ability for LWC to act as a sink for HNCO. HNCO may be a longer lived species than previously thought and exposure of this toxic molecule may pose a threat to regions with HNCO point sources like biomass burning and engine exhaust, as pointed out by Young et al. in 2012 and Barth et al. in 2013.

5 Conclusions

In summary, we provide laboratory measurements of HNCO's important thermochemical properties related to its behavior in water. We measured its Henry's Law coefficient using a bubbler column experiment to be 26 ± 2 M atm^{-1} with an enthalpy of dissolution of -34 ± 2 kJ mol^{-1}. Using ion chromatography, we determined the Arrhenius expression of HNCO's three hydrolysis mechanims: $k_1 = (4.4 \pm 0.2) \times 10^7 \exp(-6000 \pm 240 / T)$ M s^{-1}, $k_2 = (8.9 \pm 0.9) \times 10^6 \exp(-6770 \pm 450 / T)$ s^{-1} and $k_3 = (7.2 \pm 1.5) \times 10^8 \exp(-10900 \pm 1400 / T)$ s^{-1}. These values will provide better constrains on the sinks and thus lifetime of HNCO in the atmosphere with the aim of minimizing exposure of this toxic molecule.

Appendix A:

Table A1: Compilation of k_{hyd} experiments at different pH and temperatures

pH	T (K)	k_{hyd} (S^{-1})
1.75	270	$(8.30 \pm 0.64) \times 10^{-4}$
1.75	295	$(2.22 \pm 0.06) \times 10^{-3}$
1.81	283	$(1.17 \pm 0.06) \times 10^{-3}$
2.23	270	$(1.92 \pm 0.16) \times 10^{-4}$
2.23	295	$(1.39 \pm 0.02) \times 10^{-3}$
2.26	283	$(5.13 \pm 0.28) \times 10^{-4}$
2.30	295	$(1.09 \pm 0.04) \times 10^{-3}$
3.40	297	$(9.90 \pm 0.25) \times 10^{-4}$
3.91	296	$(3.74 \pm 0.03) \times 10^{-4}$
4.27	296	$(2.99 \pm 0.02) \times 10^{-4}$
5.00	296	$(6.55 \pm 0.21) \times 10^{-5}$
5.40	298	$(2.10 \pm 0.05) \times 10^{-5}$
9.26	313	$(5.39 \pm 0.26) \times 10^{-7}$
9.46	313	$(6.07 \pm 0.28) \times 10^{-7}$
10.20	313	$(6.03 \pm 0.33) \times 10^{-7}$
10.36	333	$(4.84 \pm 0.09) \times 10^{-6}$
10.37	325	$(1.70 \pm 0.09) \times 10^{-6}$

Author contribution

N.B. designed the experimental approach with critical input from J. P. D. A. and J. G. M. on the mass spectrometry method and from J. G. M. and G. R. W. on the ion chromatography method. N. B. undertook the Henry's Law experiments and B. P. conducted the HNCO hydrolysis experiments. N. B. analysed the data from both sets of experiments and N. B. wrote the manuscript with feedback from all co-authors.

Acknowledgements

References

Amell, A. R.: Kinetics of the hydrolysis of cyanic acid, J. Am. Chem. Soc., 78, 6234-6238, 1956.

Barnes, I., Solignac, G., Mellouki, A. and Becker, K. H.: Aspects of the atmospheric chemistry of amides, ChemPhysChem, 11, 3844-3857, 2010.

Belson, D. J. and Strachan, A. N.: Preparation and properties of isocyanic acid, Chem. Soc. Rev., 11, 41-56, 1982.

Beswick, H. T. and Harding, J. J.: Conformational changes induced in bovine lens a-crystallin by carbamylation, Biochem. J., 223, 221-227, 1984.

Borduas, N., Abbatt, J. P. D. and Murphy, J. G.: Gas phase oxidation of monoethanolamine (MEA) with OH radical and ozone: kinetics, products, and particles, Environ. Sci. Technol., 47, 6377-6383, 2013.

Borduas, N., da Silva, G., Murphy, J. G. and Abbatt, J. P. D.: Experimental and theoretical understanding of the gas phase oxidation of atmospheric amides with OH radicals: kinetics, products, and mechanisms, J. Phys. Chem. A, 119, 4298-4308, 2015.

Brady, J. M., Crisp, T. A., Collier, S., Kuwayama, T., Forestieri, S. D., Perraud, V., Zhang, Q., Kleeman, M. J., Cappa, C. D. and Bertram, T. H.: Real-time emission factor measurements of isocyanic acid from light duty gasoline vehicles, Environ. Sci. Technol., 48, 11405-11412, 2014.

Brownsword, R. A., Laurent, T., Vatsa, R. K., Volpp, H. -. and Wolfrum, J.: Photodissociation dynamics of HNCO at 248 nm, Chem. Phys. Lett., 258, 164-170, 1996.

Dixon, R. N. and Kirby, G. H.: Ultra-violet absorption spectrum of isocyanic acid, Trans. Faraday Soc., 64, 2002-2012, 1968.

Escorcia, E. N., Sjostedt, S. J. and Abbatt, J. P. D.: Kinetics of N_2O_5 hydrolysis on secondary organic aerosol and mixed ammonium bisulfate secondary organic aerosol particles, J. Phys. Chem. A, 114, 13113-13121, 2010.

Hocking, W. H., Gerry, M. C. L. and Winnewisser, G.: The Microwave and Millimetre Wave Spectrum, Molecular Constants, Dipole Moment, and Structure of Isocyanic Acid, HNCO, Can. J. Phys., 53, 1869-1901, 1975.

Ip, H. S. S., Huang, X. H. H. and Yu, J. Z.: Effective Henry's law constants of glyoxal, glyoxylic acid, and glycolic acid, Geophys. Res. Lett., 36, L01802, 2009.

Jensen, M., B.: On the kinetics of the decomposition of cyanic acid, Acta Chem. Scand., 12, 1657-1670, 1958.

Jones, L. H., Shoolery, J. N., Shulman, R. G. and Yost, D. M.: The molecular structure of isocyanic acid from microwave and infra- red absorption spectra, J. Chem. Phys., 18, 990-991, http://dx.doi.org/10.1063/1.1747827, 1950.

Kames, J. and Schurath, U.: Henry's law and hydrolysis-rate constants for peroxyacyl nitrates (PANs) using a homogeneous gas-phase source, J. Atmos. Chem., 21, 151-164, 1995.

Kroecher, O., Elsener, M. and Koebel, M.: An ammonia and isocyanic acid measuring method for soot containing exhaust gases, Anal. Chim. Acta, 537, 393-400, 2005.

Lee, C. K. and Manning, J. M.: Kinetics of the carbamylation of the amino groups of sickle cell hemoglobin by cyanate, J. Biol. Chem., 248, 5861-5865, 1973.

Mertens, J. D., Chang, A. Y., Hanson, R. K. and Bowman, C. T.: A shock tube study of reactions of atomic oxygen with isocyanic acid, Int. J. Chem. Kinet., 24, 279-295, 1992.

Mladenović, M. and Lewerenz, M.: Equilibrium structure and energetics of CHNO isomers: steps towards ab initio rovibrational spectra of quasi-linear molecules, Chem. Phys., 343, 129-140, 2008.

Mydel, P., Wang, Z., Brisslert, M., Hellvard, A., Dahlberg, L. E., Hazen, S. L. and Bokarewa, M.: Carbamylation-dependent activation of T cells: A novel mechanism in the pathogenesis of autoimmune arthritis, J. Immunol., 184, 6882-6890, 2010.

Poppinger, D., Radom, L. and Pople, J. A.: A theoretical study of the CHNO isomers, J. Am. Chem. Soc., 99, 7806-7816, 1977.

Rabalais, J. W., McDonald, J. R. and McGlynn, S. P.: Electronic states of HNCO, cyanate salts, and organic isocyanates. II. Absorption studies, J. Chem. Phys., 51, 5103-5111, http://dx.doi.org/10.1063/1.1671908, 1969.

Roberts, J. M., Veres, P., Warneke, C., Neuman, J. A., Washenfelder, R. A., Brown, S. S., Baasandorj, M., Burkholder, J. B., Burling, I. R., Johnson, T. J., Yokelson, R. J. and de Gouw, J.: Measurement of HONO, HNCO, and other inorganic acids by negative-ion proton-transfer chemical-ionization mass spectrometry (NI-PT-CIMS): application to biomass burning emissions, Atmos. Meas. Tech., 3, 981-990, 2010.

Roberts, J. M.: Measurement of the Henry's law coefficient and first order loss rate of PAN in n-octanol, Geophys. Res. Lett., 32, L08803, 2005.

Roberts, J. M., Veres, P. R., Cochran, A. K., Warneke, C., Burling, I. R., Yokelson, R. J., Lerner, B., Gilman, J. B., Kuster, W. C., Fall, R. and de Gouw, J.: Isocyanic acid in the atmosphere and its possible link to smoke-related health effects, Proc. Natl. Acad. Sci. U. S. A., 108, 8966-8971, 10.1073/pnas.1103352108, 2011.

Roberts, J. M., Veres, P. R., VandenBoer, T. C., Warneke, C., Graus, M., Williams, E. J., Lefer, B., Brock, C. A., Bahreini, R., Öztürk, F., Middlebrook, A. M., Wagner, N. L., Dubé, W. P. and de Gouw, J. A.: New insights into atmospheric sources and sinks of isocyanic acid, HNCO, from recent urban and regional observations, J. Geophys. Res. Atmos., 2013JD019931, 2014.

Sander, R.: Compilation of Henry's law constants (version 4.0) for water as solvent, Atmos. Chem. Phys., 15, 4399-4981, 2015.

Sander, R.: Modeling atmospheric chemistry: interactions between gas-phase species and liquid cloud/aerosol particles, Surv. Geophys., 20, 1-31, 1999.

Tsang, W.: Chemical kinetic data base for propellant combustion. II. Reactions involving CN, NCO, and HNCO, J. Phys. Chem. Ref. Data, 21, 753-791, http://dx.doi.org/10.1063/1.555914, 1992.

Tully, F. P., Perry, R. A., Thorne, L. R. and Allendorf, M. D.: Free-radical oxidation of isocyanic acid, Symp. Int. Combust., 22, 1101-1106, 1989.

Veres, P., Roberts, J. M., Burling, I. R., Warneke, C., de Gouw, J. and Yokelson, R. J.: Measurements of gas-phase inorganic and organic acids from biomass fires by negative-ion proton-transfer chemical-ionization mass spectrometry, J. Geophys. Res., 115, D23302, 2010.

Veres, P., Roberts, J. M., Warneke, C., Welsh-Bon, D., Zahniser, M., Herndon, S., Fall, R. and de Gouw, J.: Development of negative-ion proton-transfer chemical-ionization mass spectrometry (NI-PT-CIMS) for the measurement of gas-phase organic acids in the atmosphere, Int. J. Mass Spectrom., 274, 48-55, 2008.

Wang, Z., Nicholls, S. J., Rodriguez, E. R., Kummu, O., Horkko, S., Barnard, J., Reynolds, W. F., Topol, E. J., DiDonato, J. A. and Hazen, S. L.: Protein carbamylation links inflammation, smoking, uremia and atherogenesis, Nat. Med., 13, 1176-1184, 2007.

Wentzell, J. J. B., Liggio, J., Li, S., Vlasenko, A., Staebler, R., Lu, G., Poitras, M., Chan, T. and Brook, J. R.: Measurements of gas phase acids in diesel exhaust: a relevant source of HNCO?, Environ. Sci. Technol., 47, 7663-7671, 2013.

1 Woodward-Massey, R., Taha, Y. M., Moussa, S. G. and Osthoff, H. D.: Comparison of
2 negative-ion proton-transfer with iodide ion chemical ionization mass spectrometry for
3 quantification of isocyanic acid in ambient air, Atmos. Environ., 98, 693-703, 2014.

4 Young, P. J., Emmons, L. K., Roberts, J. M., Lamarque, J., Wiedinmyer, C., Veres, P. and
5 VandenBoer, T. C.: Isocyanic acid in a global chemistry transport model: tropospheric
6 distribution, budget, and identification of regions with potential health impacts, J. Geophys.
7 Res., 117, D10308, 2012.

8 Yu, S., Su, S., Dorenkamp, Y., Wodtke, A. M., Dai, D., Yuan, K. and Yang, X.: Competition
9 between direct and indirect dissociation pathways in ultraviolet photodissociation of HNCO,
10 J. Phys. Chem. A, 117, 11673-11678, 2013.

11 Zhao, R., Lee, A. K. Y., Wentzell, J. J. B., Mcdonald, A. M., Toom-Sauntry, D., Leaitch, W.
12 R., Modini, R. L., Corrigan, A. L., Russell, L. M., Noone, K. J., Schroder, J. C., Bertram, A.
13 K., Hawkins, L. N., Abbatt, J. P. D. and Liggio, J.: Cloud partitioning of isocyanic acid
14 (HNCO) and evidence of secondary source of HNCO in ambient air, Geophys. Res. Lett., 41,
15 6962-6969, 2014.

16